Marine Geology 291-294 (2012) 162–175

Contents lists available at ScienceDirect

Marine Geology

journal homepage: www.elsevier.com/locate/margeo

Morphodynamics of an anthropogenically altered dual-inlet system: John's Pass and Blind Pass, west-central Florida, USA

Ping Wang [a,*], Tanya M. Beck [b]

[a] Department of Geology, University of South Florida, Tampa, FL 33620, USA
[b] U.S. Army Engineer Research and Development Center, Coastal and Hydraulics Laboratory, Vicksburg, MS 39180, USA

ARTICLE INFO

Article history:
Received 20 July 2010
Received in revised form 19 May 2011
Accepted 1 June 2011
Available online 6 June 2011

Keywords:
coastal morphodynamics
nearshore sediment transport
barrier islands
tidal inlets
ebb tidal delta
flood tidal delta
tides
waves
Florida

ABSTRACT

The morphodynamics of the John's Pass–Blind Pass dual inlet system were investigated based on hydrodynamic and morphology measurements, and numerical modeling. The co-existence of the dual inlets is realized by the dominance of mixed-energy John's Pass in terms of tidal prism and size of the ebb delta and the artificial maintenance of the wave-dominated migratory Blind Pass. Due to the secondary role of Blind Pass, the aggressive anthropogenic activities there do not seem to have a significant influence on the morphodynamics of John's Pass. On the other hand, the opening (in 1848) and subsequent evolution of John's Pass had substantial influence on Blind Pass, causing it to migrate rapidly to the south. In addition, anthropogenic activities had much more influence on the morphodynamics of the secondary Blind Pass than that of the dominating John's Pass.

Results from numerical modeling provide a semi-quantitative understanding of the hydrodynamics and morphodynamics of John's Pass and Blind Pass in association with cold front passages, which have substantial influences on inlet morphology. Two large eddies are modeled from the interactions between the southward longshore current and John's Pass ebb and flood flow, respectively. These eddies are closely related to the morphodynamics of the channel margin linear bar and longshore transport divergence at the downdrift side. Both are key features of a mixed-energy inlet. The shallow water and wave-breaking-induced longshore current and elevated sediment suspension along the ebb delta terminal lobe provide the pathway for sediment bypassing. The morphodynamics of Blind Pass are dominated by wave forcing. The weak ebb jet is not capable of forming a sizable ebb delta and tends to be deflected by the strong longshore current, causing elevated longshore transport along the downdrift beach. The 90-degree turn of the inlet, which is common for wave-dominated migratory inlets, results in weak ebb flushing along the updrift (north) side of the inlet, and is responsible for the alongshore migration of the inlet before the artificial stabilization and sedimentation along the northern side of the inlet following stabilization.

1. Introduction

Tidal inlets provide a link between the coastal ocean and back-barrier bay, exchanging water, sediment, nutrients, and other materials between them. Natural sediment supply for an inlet system can be from the land via rivers and estuaries, offshore, and alongshore. Sediment transport through and in the vicinity of tidal inlets is active and complicated, driven by interactive hydrodynamic forcing including tidal currents, breaking and non-breaking waves, wave-driven currents, wind-driven currents, and fluvial currents. Tidal inlet morphology is highly variable, ranging from deep channels to shallow shoals, and with a variety of bedforms across the ebb- and flood-tidal deltas (FitzGerald, 2011). Interactive morphological features associated with a tidal inlet system typically include a main channel between the barrier islands, an ebb-tidal delta complex, a flood-tidal delta complex, and adjacent beaches and spit complexes (Hayes, 1979; FitzGerald, 1996, 2011). Depending on the relative dominance of tide and wave forcing, tidal inlet systems can be classified as tide-dominated, wave-dominated, and mixed energy (Hayes, 1979; Davis and Hayes, 1984; Davis, 1994). Generally, tidal forcing tends to maintain a deep and straight inlet channel for efficient tidal exchange. Wave forcing tends to transport sediment alongshore, resulting in infilling of the inlet channel and causing the inlet to migrate in the downdrift direction (Bruun, 1978). The morphodynamics of tidal inlets reflect the dynamic balance between tidal forcing and wave forcing. A tide-dominated inlet has a deep and straight main channel with a well developed ebb-tidal delta characterized by large, shore-perpendicular channel margin linear bars (Davis, 1994). A wave-dominated inlet tends to be migratory with a small ebb-tidal delta or none at all. A tide-dominated inlet tends to have a relatively large tidal prism, whereas a wave-dominated inlet typically has a relatively small tidal prism (Davis, 1994). Two kinds of mixed-energy inlets are distinguished:

* Corresponding author. Tel.: +1 813 974 9170; fax: +1 813 974 2654.
E-mail address: pwang@usf.edu (P. Wang).

0025-3227/$ – see front matter © 2011 Elsevier B.V. All rights reserved.
doi:10.1016/j.margeo.2011.06.001

mixed-energy offset inlets and mixed-energy straight inlets (Davis, 1994). A mixed-energy offset inlet is characterized by a modest ebb-tidal delta and a distinct downdrift offset in the shoreline, whereas a mixed-energy straight inlet has an ebb-tidal delta bending toward the downdrift without significant shoreline offset (Gibeaut, 1991). For the dual-inlet system examined here, John's Pass is a mixed-energy straight inlet and Blind Pass is a wave-dominated inlet.

Many inlets also support artificially maintained navigation channels, further complicating the system by introducing substantial anthropogenic controls (Kraus, 2009). Dean (1988) concluded that more than 80% of the beach erosion issues along the Florida coast can be directly linked to tidal inlets. Rapid and large morphological changes are often measured at tidal inlets, tidal deltas, and their adjacent beaches, making them one of the most dynamic systems in the nearshore environment. Therefore, understanding and quantifying the morphodynamics of tidal inlets is a challenging task.

Many bays along the microtidal, mixed energy west-central Florida coast are served by more than one tidal inlet (Davis, 1994). If the multiple inlets are relatively close to each other, the hydrodynamic and morphologic change at one inlet can be directly influenced by the evolution of the other inlets (Van de Kreeke, 1990; Aubrey and Giese, 1993; FitzGerald, 1993; Fitzgerald, 1996; Van de Kreeke, et al., 2008; Pacheco et al., 2010). Numerous studies have been conducted to examine the hydrodynamics and co-existence of multiple inlets (e.g., Van de Kreeke, 1990; Salles et al., 2005; Van de Kreeke et al., 2008; Pacheco et al., 2010); however, morphodynamic interactions between adjacent inlets are not well understood. In addition, most of the west-central Florida inlets are heavily modified anthropogenically. Engineering activities at one inlet can significantly influence the morphodynamics of another. Typical engineering activities at a tidal inlet include construction of jetties, channel dredging, ebb-tidal delta mining, construction of causeways and artificial islands in the back-bay, and nourishment of adjacent beaches. In the case of the west-central Florida coast, the co-existence of multiple inlets is at least partially artificially maintained. The morphodynamics of the John's Pass and Blind Pass system are influenced by nearly all the natural and anthropogenic factors discussed above.

In this study, the John's Pass and Blind Pass morphodynamics are examined through analysis of data from field measurements and numerical modeling. Time-series aerial photos from 1926 were compared to examine large-scale morphological changes. Bathymetric surveys, along with flow and wave measurements, were conducted to link the hydrodynamics to morphological changes. The state-of-the-art numerical model, Coastal Modeling System (CMS), is employed to examine the spatial patterns of current, wave, and sediment transport. The CMS was developed by the US Army Engineer Research and Development Center's (ERDC) Coastal Inlets Research Program (CIRP) specifically for integrated numerical modeling of hydrodynamics (Buttolph et al., 2006; Lin et al., 2011; Reed et al., 2011; Wu et al., 2011), sediment transport (Larson et al., 2011), and morphologic changes (Sanchez and Wu, 2011) associated with tidal inlets.

The objectives of this study are to examine: 1) morphodynamics of an interactive dual-inlet system; 2) factors controlling the morphodynamics of the inlets, evaluated on the basis of both field data and simulated data from the CMS; 3) anthropogenic influences on the morphodynamics of the two inlets; and 4) sediment pathways controlling the morphodynamics of the inlet system.

2. Study area

John's Pass and Blind Pass, separated by the 6-km long Treasure Island, service a portion of Boca Ciega Bay along the west-central Florida coast (Fig. 1). Regionally, the John's Pass–Blind Pass system is part of the west-central Florida barrier-island chain that extends north from the mouth of Tampa Bay. The entire area, from the beaches to the inlets to the back-bay, is densely developed since the 1930s. Several causeways and bridges and numerous dredge and fill finger channels dissect the back-barrier bay, especially within the water body landward of Blind Pass (Fig. 1).

The overall wave energy along this coast is mild with average breaker heights for west-central Florida estimated to be 0.25–0.30 m (Tanner, 1960). Nearshore waves approximately 400 m offshore Blind Pass were measured from November 25, 2003 to February 26, 2005. A total of 4181 measurements were obtained with a measurement interval of 1.5 h. This yields roughly 261 days of wave data (Fig. 2). The average significant wave height was 0.26 m with an average peak wave period of 5.8 s. The influences of cold-front passages are apparent, as illustrated by the frequent high wave events during the winter season from October to March. The spring season (March and April) can have relatively high wave energy induced by the passage of late cold fronts. The summer of 2004 was exceptional in that the passage of three tropical storms in September and October, Frances, Ivan and Jeanne (Elko and Wang, 2007) resulted in three substantial, high-wave events. The distal passage of Hurricane Ivan generated long-period (12–16 s) swells (Fig. 2, lower), which are rare for this coast. Although representing a short period of time, Fig. 2 illustrates the typical pattern of wave conditions, with the exception of the three tropical storms. Consequent to the wave conditions, sediment transport in the study area tends to be episodic as it is controlled by high-energy events typically associated with the frequent passages of winter cold fronts (Walton, 1973; Davis, 1997; Elko et al., 2005; Elko and Wang, 2007). Sustained wind and waves during these events tend to come from a northerly direction, driving a net southward longshore sediment transport.

The study area is characteristic of a mixed tidal regime. The spring tide is typically diurnal with a range of roughly 0.8 to 1.2 m, whereas the neap tide is semi-diurnal with a range of 0.4 to 0.5 m (Fig. 3). Although the spring tide tends to be diurnal, a short pause or slight water-level fall typically occurs during the prolonged flooding phase, whereas the shorter ebbing phase is typically not interrupted. The magnitude of the slight water-level fall during the spring flooding phase increases as the tidal cycle changes to a neap tidal cycle, and eventually becomes a semi-diurnal tide during the neap phase (Fig. 3). The tides measured in the offshore (seaward of John's Pass at the edge of Fig. 1), John's Pass channel, Blind Pass channel, and inside the bay (next to the St. Pete Beach Causeway; Fig. 1) matched well in terms of both tidal range and phase, indicating that the relatively small system and bay interconnectivity did not produce a considerable tidal phase lag (Fig. 3). However, a noticeable phase lag between the tides measured in the back-bay and the tides at the other three locations was observed toward the end of the deployment in early August (Fig. 3, right end). This was caused by the storm surge associated with the passage of Tropical Storm Faye.

Sediments along the west-central Florida coast are bimodal composed of siliciclastic and carbonate fractions. The siliciclastic component is primarily fine quartz sand with a mean grain size of 0.17 mm. The carbonate fraction is mostly shell debris of various sizes. Mean grain size in the study area varies typically from 0.2 mm to 1.0 mm, controlled by the varying amounts of shell debris. The largest grain sizes are found in the channel thalweg where coarse lag deposits are concentrated.

John's Pass is a jettied inlet located between Treasure Island to the south and Sand Key to the north. Since its opening in 1848 by a hurricane, John's Pass has gradually become the dominant inlet of the John's Pass–Blind Pass system, capturing 70–80% of the tidal prism (Mehta et al., 1976). As shown in Fig. 1, the portion of Boca Ciega Bay landward of John's Pass is larger and not as dissected by man-made islands as compared to the portion landward of Blind Pass. Time-series aerial photos show that substantial anthropogenic activities at John's Pass started in the 1950s (Fig. 4). Three of the significant

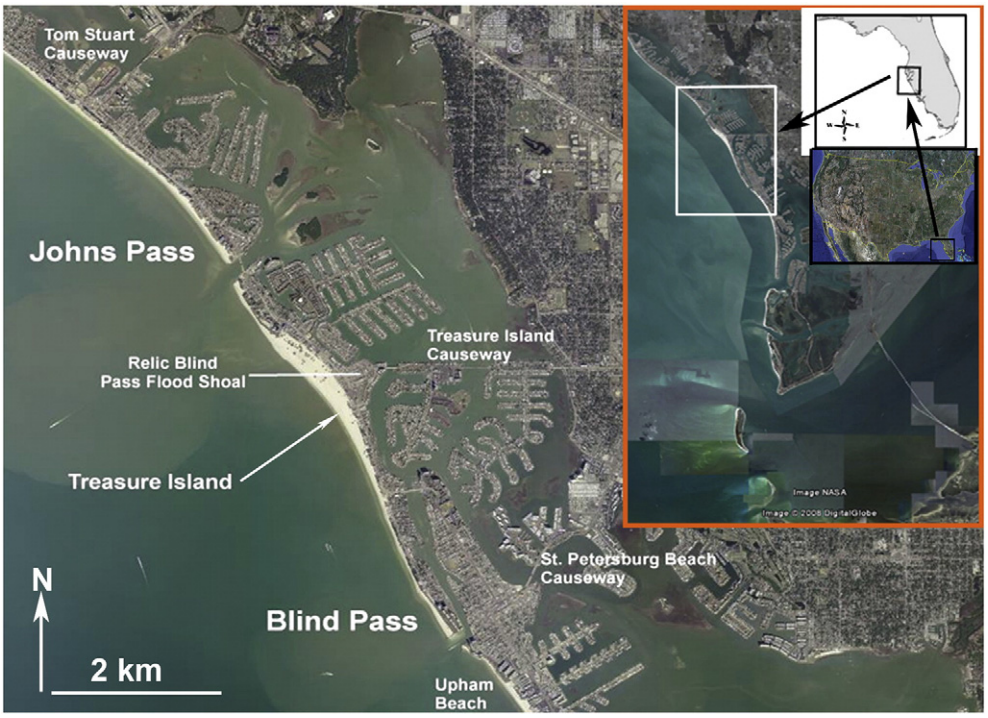

Fig. 1. The John's Pass and Blind Pass inlet system, illustrated with a 2004 aerial photograph. The long spit and relic Blind Pass flood-tidal delta (shoal) indicates the southward migration of the inlet.

engineering activities at John's Pass include: 1) construction and extension of the inlet jetties along both sides, 2) construction of numerous artificial islands (aka, finger channels) in the back-barrier bay, and 3) a nearshore berm nourishment (~1970), which was artificially moved onshore and attached to the shoreline in 1974. Also apparent from the time-series aerial photos, the shoreline positions in

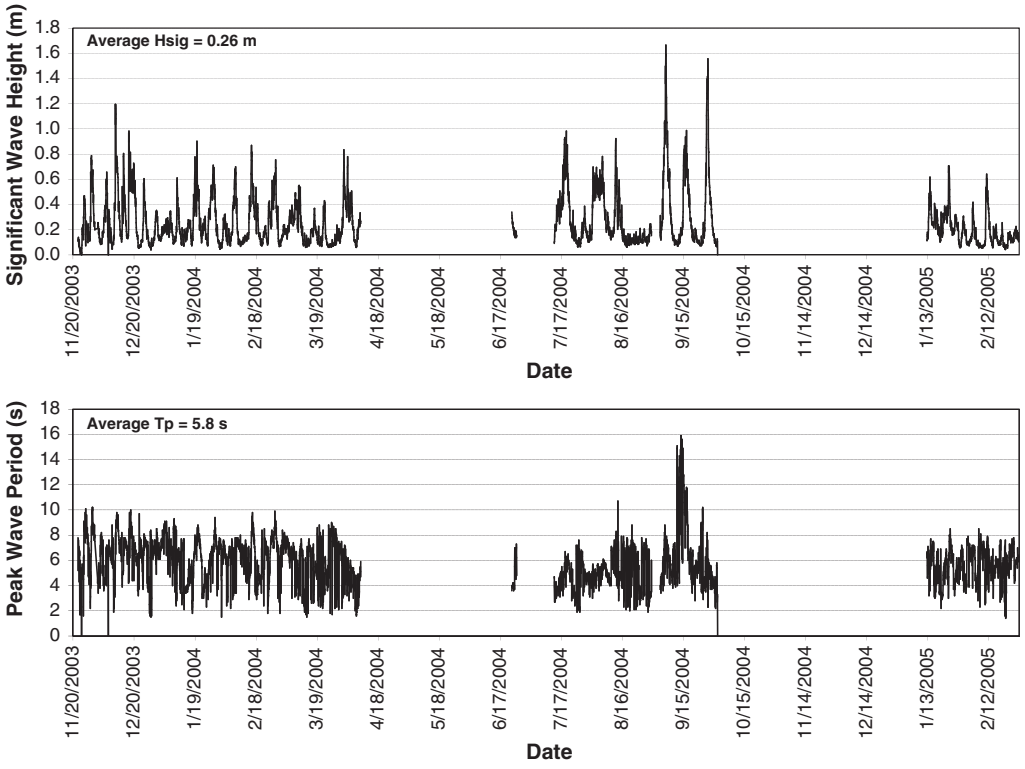

Fig. 2. Wave conditions measured at ~400 m offshore Upham Beach at 4 m water depth. The measurements were conducted from November 25, 2003 to February 26, 2005 with some gaps in time due to equipment maintenance. A total of 4181 measurements were obtained representing roughly 261 days. Upper panel: significant wave height. Lower panel: peak wave period.

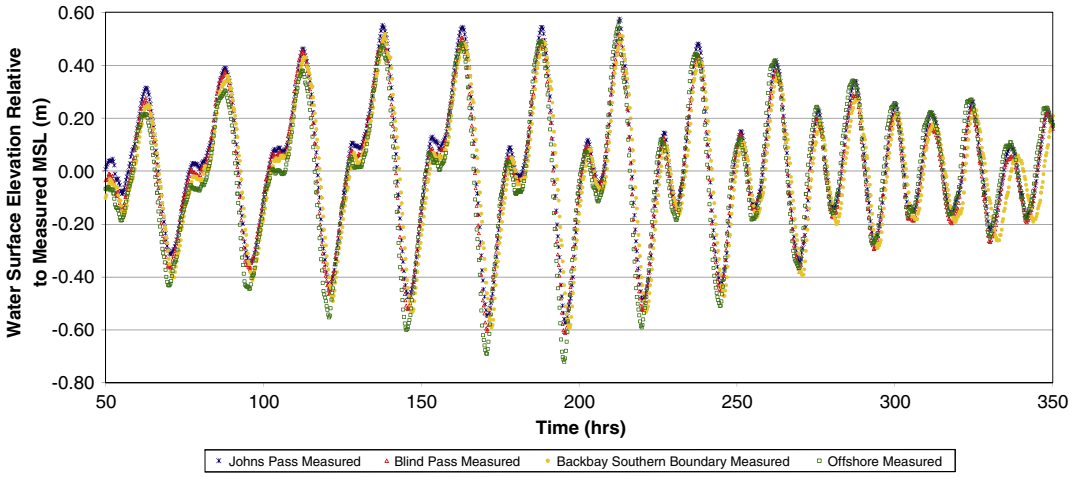

Fig. 3. Measured tides from July 23, 2008 to August 5, 2008 at four locations including: offshore area (seaward of John's Pass at the edge of Fig. 1), John's Pass channel, Blind Pass channel, and inside the bay (next to the St. Pete Beach Causeway) (Fig. 1). Similar tide conditions were measured throughout the inlet system. Note the phase lag of the back-bay measurement (right end of the graph), which is associated with the passage of Tropical Storm Faye in August 2008.

the vicinity of the inlet varied substantially. Except for vegetation changes, the flood-tidal delta has remained largely stable. John's Pass is characteristic of a mixed-energy straight inlet with a large ebb-tidal delta, skewed to the south in the direction of the southward net longshore sediment transport (Fig. 5). The channel-margin linear bar along the updrift (north) side, the relatively shallow terminal lobe, and the swash bar complex over the downdrift portion of the ebb-delta are illustrated by the detailed bathymetry. The downdrift attachment point where the bypassed sediment reaches the beach is outlined by the protruding shoreline (Fig. 6). The Sunshine Beach, updrift (north) of the attachment point (Fig. 6 middle), experiences chronic erosion, whereas the beach downdrift (south) of the attachment point is wide with up to 300 m of dry beach, and has shown an accretionary trend over the last two decades. John's Pass and its ebb-tidal delta have been dredged in 1960, 1961, 1966, 1971, 1980, 1985, 1988, 1991, and 2000 (Barnard, 1998). The dredged sand is typically used to nourish the adjacent beaches.

The origin of Blind Pass is not historically recorded. Prior to the opening of John's Pass in 1848, Blind Pass appeared to have been the dominant inlet serving Boca Ciega Bay, having large flood- (Fig. 1) and ebb-tidal deltas. As John's Pass gradually captured a substantial portion of the tidal prism, the net longshore sediment transport caused rapid southward migration of Blind Pass (Davis and Barnard, 2003), as illustrated by the long southward migrating spit (Figs. 1 and 7). Blind Pass was eventually stabilized with jetties constructed in 1937, fixing the entrance channel into a sharp 90-degree turn with a relatively wide (160 m) entrance channel (Fig. 7). Similar to John's Pass, extensive dredge-and-fill construction was conducted in the back-barrier bay between the 1940s and 1960s (Figs. 1 and 7). The engineered islands, as well as the construction of several causeways, resulted in an approximately 30% reduction of the back-bay area and thus a continued decrease in tidal prism (Davis and Barnard, 2000, 2003). The gradual "takeover" of John's Pass since its opening in 1848 and the artificial reduction of the bay area have resulted in substantial

Fig. 4. Time-series aerial photos of John's Pass from 1926 to 2010. Note the relatively stable flood tidal delta, the shoreline variation near the inlet, and the nearshore berm nourishment shown on the 1970 photo.

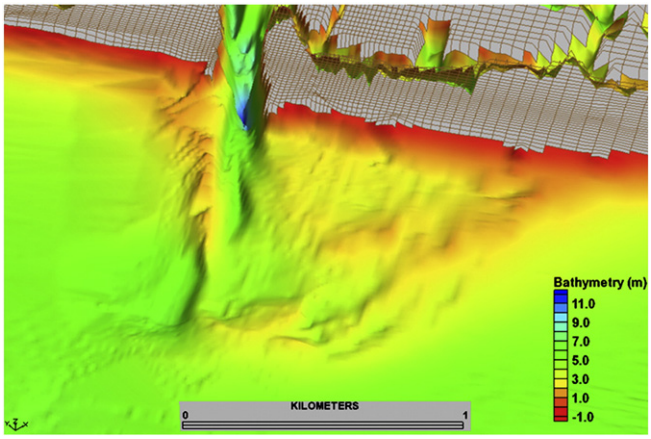

Fig. 5. The John's Pass ebb-tidal delta survey from 2008. Depths (positive number) are relative to mean sea level. The ebb delta is skewed to the south, controlled by the southward longshore sediment transport. Note the complicated bathymetry with numerous swash bars.

morphodynamic responses at Blind Pass. The Blind Pass ebb-tidal delta, apparent on the 1926 photo (Fig. 7), diminished and is completely absent in the 1985 photo and thereafter. The ebb delta became unstable and migrated downdrift to amalgamate with the beach as shown in the 1957 photo (Fig. 7). This process serves as an episodic mechanism of sediment bypassing across the tidal inlet, in contrast to gradual bypassing as observed at the John's Pass attachment point (Fig. 6). Episodic onshore migration and amalgamation of the ebb-tidal delta can be caused by a decreasing tidal prism as in the case of Blind Pass, or in response to natural or artificial channel realignment (FitzGerald, 1984). The wide downdrift beach seen on the 1957 photo was rapidly eroded by the southward longshore transport, as part of the bypassing process. Constructions of several large buildings co-incidental with the ebb delta amalgamation and the subsequent beach erosion converted the downdrift Upham Beach into a severe erosional hot spot (Elko and Wang, 2007).

The wide entrance channel relative to the small tidal prism at Blind Pass has become an effective trap for the southward longshore transport, as shown in the 1985 and 2004 aerial photos (Fig. 7).

Fig. 6. The attachment point of the John's Pass ebb-tidal delta, where bypassed sand reaches the downdrift shoreline. Note the wide beach at the attachment point, the narrow Sunshine Beach north of the attachment point, and the wide beach south of the attachment point. The photo was taken in 2008 looking south.

Without the ebb delta, little to no sand would bypass to the downdrift beach, resulting in severe erosion, as shown in 1985, 1995, and 2004 aerial photos (Fig. 7). Dredging operations were conducted in 1937, 1964, 1969, 1975, 1979, 1983, 1990, and 2000 to maintain the entrance channel at Blind Pass. The dredged sand was used to nourish adjacent beaches, particularly the chronically eroding downdrift Upham Beach. Overall, the morphology of Blind Pass was significantly influenced by the opening and subsequent evolution of John's Pass, in addition to the intense engineering activities.

3. Materials and methods

3.1. Field data collection

A series of field investigations was conducted at John's Pass and Blind Pass since 2001. A large amount of the field measurements was concentrated at the main channel of Blind Pass after the last channel dredging in the summer of 2000. Time-series bathymetric surveys were conducted roughly quarterly from August 2002 to June 2004 using the combination of a precision echo-sounder for depth and a synchronized Real-Time-Kinematic (RTK) Global Positioning System (GPS) for position. In addition, monthly level-and-transit surveys using an electronic total station were conducted from February 2003 to February 2004. The monthly survey of 9 lines over the northern shoal was designed to capture the infilling rate and pattern over this active shoaling area (Fig. 8). All surveys are referenced to NGVD29, which is roughly 0.15 m below mean sea level in this area.

Several flow measurements were conducted at the John's Pass and Blind Pass system. The first series of flow measurements was conducted in the winter of 2001. Two upward-looking Acoustic Doppler current Profilers (ADP) were deployed simultaneously in the channel thalweg of John's Pass and Blind Pass near the inlet mouths. The goal was to compare flow velocities at the two interactive inlets and to calculate the tidal prism. The second series of flow measurements was conducted between 2002 and 2003 using an upward-looking ADP in combination with a side-looking ADP, thereby measuring flow patterns both through the water column and across the channel. The flow measurements were conducted at two locations with one near the mouth and one near the bend, each for approximately one month (Fig. 8). The quasi 3-D flow data was to provide insight into the sediment transport pattern in the Blind Pass channel. The third series of flow measurements was conducted in the summer of 2008. An offshore wave-tide gage and three tide gages in the inlets and back-bay were deployed. The goals of the 2008 measurements were to provide input conditions for the numerical model and to verify the modeling results. Overall, the goals of the field measurements were two-fold: 1) to quantify the morphodynamic processes at the dual inlet system, and 2) to verify and calibrate the numerical model.

3.2. Numerical modeling using the Coastal Modeling System (CMS)

The CMS is a process-based suite of models that integrate hydrodynamics, sediment transport, and morphologic change through the coupling of two modules, CMS-Flow and CMS-Wave. The CMS was developed specifically for modeling inlet processes and morphology changes. CMS-Flow solves depth-integrated continuity and momentum equations using a finite-volume method (Kraus and Militello, 1999; Buttolph, et al., 2006; Reed et al., 2011). Both CMS-Flow and CMS-Wave have been tested extensively for inlet applications at numerous locations. Generally, the calculated tidal-driven flow velocity and wave field matched the measured values well (e.g., Beck and Kraus, 2011; Lin et al., 2011; Reed et al., 2011). In this study, the CMS is applied to semi-quantitatively illustrate regional patterns of wave–current interaction and sediment transport in relation to inlet morphodynamics. CMS-Flow results for water level and current

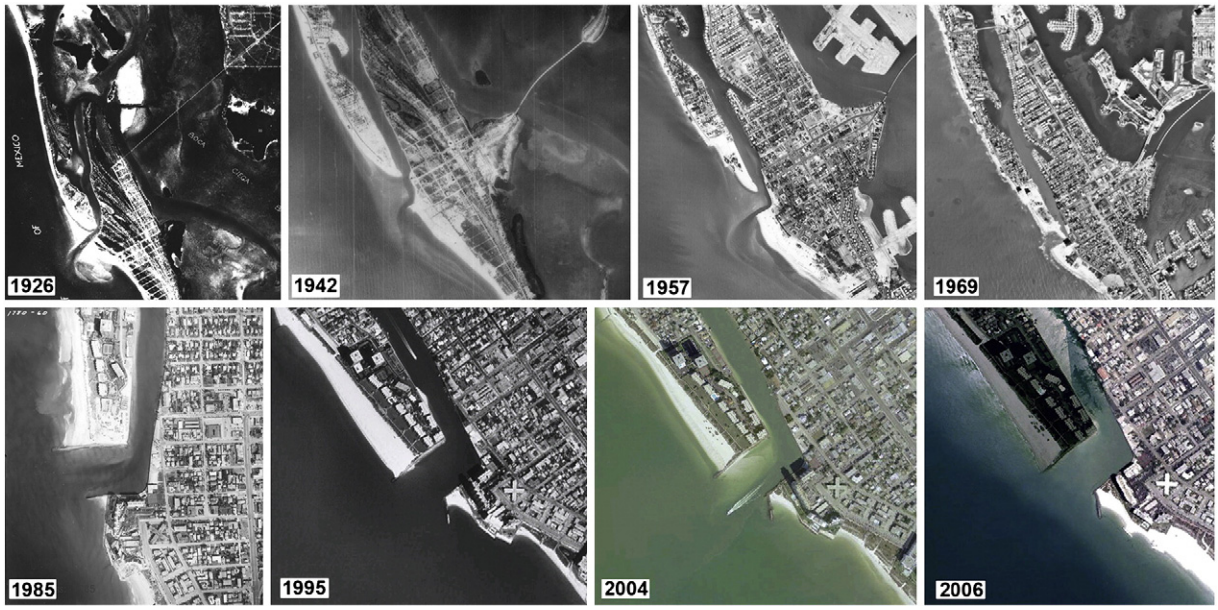

Fig. 7. Time-series aerial photos of Blind Pass from 1926 to 2006. Note the diminishment of the ebb-tidal delta over the years and the severe beach erosion at the downdrift.

were compared and validated for the measurement sites. Validation of the individual hydrodynamics parameters (such as wave height) and sediment transport parameters is not directly related to the regional semi-quantitative morphodynamics discussions here.

The unified sediment transport formula, Lund-CIRP (Camenen and Larson, 2007; Larson et al., 2011), and a non-equilibrium transport formula (NET) (Wu, 2008; Sanchez and Wu, 2011) were applied for the computation of sediment transport and morphology change. The sediment transport computation included transport of non-cohesive sediments by both currents and waves (non-breaking and breaking waves). Given the large areas of shallow water typically associated with tidal inlets, e.g. over the ebb-tidal delta and near the shoreline, an accurate representation of wave breaking and the subsequent elevated sediment suspension and transport is essential.

CMS-flow (Reed et al., 2011) is coupled with CMS-Wave (Lin et al., 2011), which is a steady-state, spectral transformation wave model.

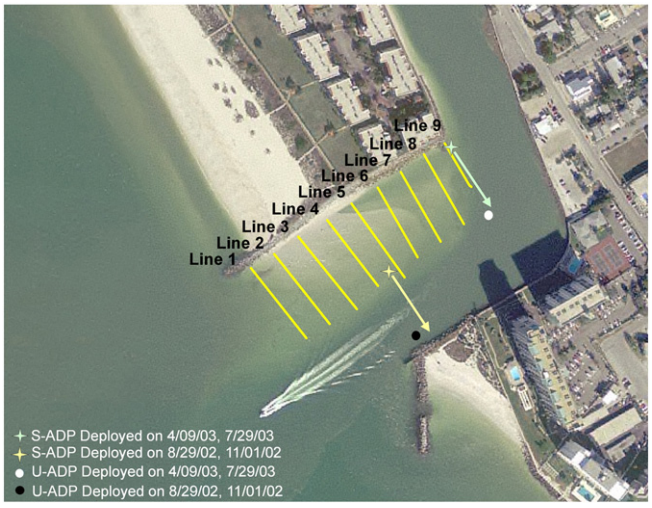

Fig. 8. Monthly survey lines across the Blind Pass northern shoal, and locations and times of current meter deployments. UADP: upward-looking Acoustic Doppler current Profiler; SADP: side-looking Acoustic Doppler current Profiler.

CMS-Wave is an improved and modified version of the wave model WABED for inlet applications with options to include several different structures (Mase and Kitano, 2000; Mase, 2001; Mase et al., 2005; Lin et al., 2006, 2008). The model computes wave refraction, shoaling, reflection, diffraction, and breaking. The radiation stress induced by breaking is computed and passed to CMS-Flow for the calculation of the wave-induced longshore current, in addition to wave height, period, and setup, all of which are necessary for calculating sediment transport under combined waves and currents.

An accurate bathymetric grid is essential because wave propagation is strongly influenced by nearshore bathymetry. In addition, high spatial resolution is necessary to adequately resolve the inlets. The nearshore, the two inlets, the back-barrier bay, and adjacent beaches were surveyed between 2006 and 2008. Data from the NOAA NGDC Coastal Relief Model (http://ngdc.noaa.gov) covered the offshore regions that were not surveyed by this study. The CMS grid was constructed based on the above bathymetric data (Fig. 9). A variable-sized rectangular-cell grid system, with a spatial resolution ranging from 10×10 m in the vicinity of the channels, the ebb-tidal deltas, and the nearshore zone, to 80×100 m near the ocean boundary was generated with the main axes (oriented along 35°–215°) parallel to the regional shoreline and bathymetric trend. The large depth variations associated with deep channels, and shallow flood- and ebb-tidal deltas are apparent.

To simulate the flow field, CMS-Flow was driven by the measured tide at the offshore boundary. It is assumed that a 4-week record measured during July–August 2008 can adequately represent the offshore tidal variation (Fig. 3). The 4-week record was therefore replicated to cover a 2-year period. The WIS (Wave Information Study) hindcast data, developed by the U.S. Army Corps of Engineers (USACE), was used to provide a continuous wave record. The closest WIS station is located approximately 30 km offshore John's Pass at 17-m water depth, or about 27 km seaward of the ocean boundary. Snell's Law was applied to transform waves from the 17 m water depth to the seaward boundary of the modeling domain. After examining a 20-year (1980–1999) WIS record, waves during two years, 1997 and 1999, were judged to be representative and used in the modeling effort. Since the WIS hindcast wave data was computed based on regional wind forcing, it was, therefore, not considered again in the wave-propagation modeling to avoid over-prediction. Although CMS-Wave

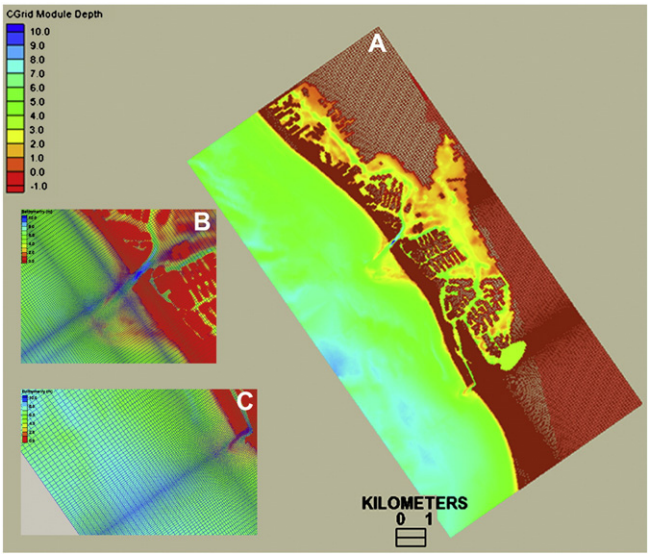

Fig. 9. The model domain of the John's Pass and Blind Pass system. Depths (positive) are relative to mean sea level. The insets illustrate the refined dense grid in the inlet channels and over the ebb deltas.

is a full-plane model, the half-plane alternative was selected for this study. This is based on: 1) the model grid is oriented approximately parallel to the NW–SE trending shoreline, and 2) this stretch of coast does not experience highly oblique incident waves due to the refraction by the wide and gently sloping inner shelf. In addition, it is reasonable to assume that offshore-directed waves should not have significant influence on beach-inlet morphology and can therefore be neglected in the modeling. A spatially constant grain size of 0.26 mm, roughly representing the average size of a large number of samples, was used. Although a nearly 2-year morphology change was produced, this study focuses on the spatial pattern of current, wave, and sediment transport for the analysis of morphodynamics. Detailed comparison between the predicted morphologic changes and measured ones is beyond the scope of this paper.

4. Results and discussion

In the following, the morphodynamics of the John's Pass and Blind Pass system are discussed based on field data and the results from the numerical modeling. The simulated flow, wave, and sediment transport fields provide insight into the interpretation of the observed morphodynamics at the dual inlets.

4.1. Measured tidal currents through the inlet channel

Simultaneous flow measurements through the channel thalweg were conducted in 2001. Much faster flow was measured through John's Pass than through Blind Pass, especially during the flooding tide (Fig. 10). The peak ebb velocity through the 200-m wide John's Pass approaches 1.5 m/s versus about 1.0 m/s through the 160-m wide Blind Pass. The peak flood velocity through John's Pass reaches 1.2 m/s, whereas the flood velocity is mostly less than 0.5 m/s at Blind Pass. The high flow velocity combined with the larger cross-sectional area (Barnard, 1998) yielded a much larger tidal prism at John's Pass than at Blind Pass, confirming that the John's Pass inlet is the dominant inlet of the two, as suggested by Mehta et al. (1976). The strong flow through John's Pass is also responsible for the relatively deep and straight inlet channel and the large ebb-tidal delta. Flow velocity through most of the water column is largely homogeneous (Fig. 11), suggesting that a depth-averaged model like CMS should provide a reasonable representation of hydrodynamics at John's Pass and Blind Pass.

Tidal flow velocity exhibits substantial variation across the Blind Pass channel. In addition, the cross-channel distribution pattern differs between ebb and flood tide (Fig. 12). During ebb tide, the flow velocity measured at the channel thalweg is 2 to 3 times larger than that measured over the north shoal (Fig. 12A; Fig. 8 for location). The peak ebb velocity through the channel thalweg approaches 1.0 m/s. During flooding tide, the flow velocity is primarily uniform across the channel, peaking at about 0.5 m/s. The flow patterns measured across the channel near the bend (Fig. 12B, Fig. 8 for location) are different from those measured near the entrance. Both the flood and ebb velocity show a decreasing trend toward the channel bend where sedimentation was measured. For this particular tidal cycle, the peak ebb velocity is nearly 1.2 m/s. The smaller peak flood velocity relates to the characteristics of the spring tides, which tend to have a prolonged rising phase followed by a sharp falling phase (Fig. 3). The documented tidal flow pattern across the inlet channel can be attributed to the nearly 90-degree turn. The northern side of the inlet lies in the shadow zone of the ebb current as it turns around the corner. Such a sharp bend is common for migratory inlets, resulting from extension of the updrift barrier-island and recession of the downdrift side. Therefore, the tidal flow distribution shown in Fig. 12 should be representative of many wave-dominated migratory inlets. For the mixed-energy straight John's Pass, flow is largely uniform across almost the whole channel.

4.2. Measured morphological changes at Blind Pass and John's Pass

As discussed earlier, the morphological features at John's Pass and Blind Pass are quite different, reflecting the relative dominance of tides and waves. John's Pass is the dominant inlet of the two and remains relatively stable, whereas the weaker Blind Pass responds more actively to changes at John's Pass and anthropogenic activities. A major morphological feature of Blind Pass is the infilling between the structured channel and the severe erosion along the downdrift Upham Beach. A field study aimed at quantifying sedimentation in the Blind Pass channel was conducted after the dredging in the summer of 2000 (Wang et al., 2007). Three years after the dredging occurred, the northern side of the inlet had filled to a level less than 1 m below mean sea level from the cut depth of about 5 m. Recently, an ebb-tidal delta has developed with a west–southwest trending orientation (Fig. 13). By 2008, i.e. eight years after the last dredging, the ebb-tidal delta had become relatively substantial in size with visible wave shoaling and breaking along much of the delta during both fair and stormy weather. The development of the ebb-tidal delta at this wave-dominated inlet was influenced by the sand introduced to the nearshore system by the beach nourishments of 2004 and 2006 on Treasure Island and Long Key (Wang et al., 2008), located north and south of the inlet, respectively. The ebb-tidal delta may thus not be maintained by natural wave-dominated conditions alone.

Based on time-series survey data, the shoaling rate in the entrance channel of Blind Pass was 35,000 m^3/year during the first two years, reducing to 26,000 m^3 in the third year probably due to sediment bypassing around the corner into the back channels (Wang et al., 2007). The inlet effectively serves as an efficient trap for sediment supplied by southward longshore transport. Most of the sediment shoaling occurs along the north side of the inlet. This corresponds to 1) its proximity to the sand source, 2) limited impoundment at the north jetty, 3) weak ebb flushing due to preferential location of the ebb jet along the south side, and 4) relatively stronger flood current in comparison to the ebb current along the north side (Figs. 11 and 12). Accumulation and erosion patterns in the Blind Pass channel demonstrate a distinct seasonal trend, with typically active sedimentation in the winter driven by frequent cold front passages and sediment redistribution during the calmer summer season (Fig. 14).

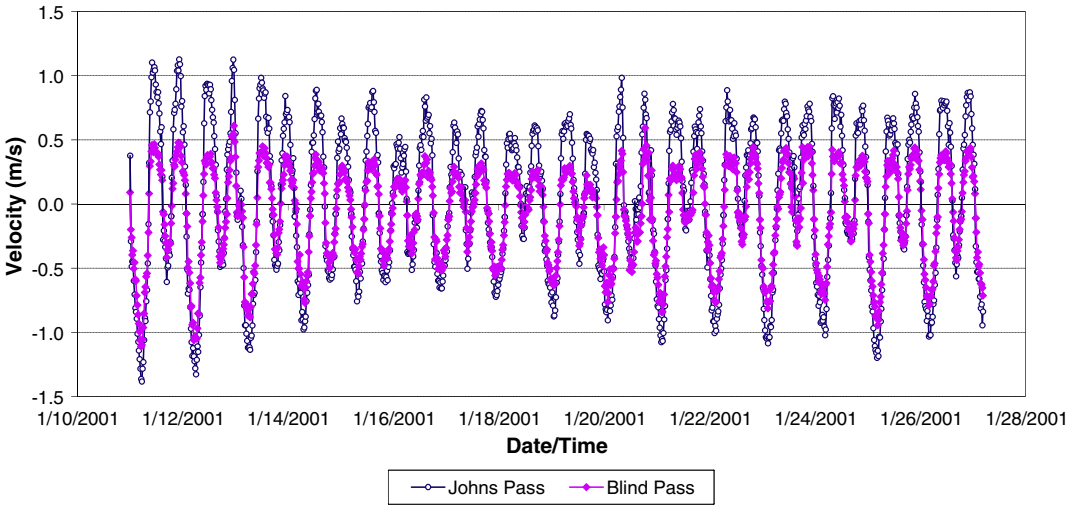

Fig. 10. Measured flow velocity through the main channels of John's Pass and Blind Pass. Negative velocity represents ebb flow and positive represents flood flow.

The channel infilling took the form of a distinct sediment body, with the deposition occurring near the mouth at the beginning of the winter season and migrating further into the inlet during late winter and early summer.

Upham Beach, directly south and downdrift of Blind Pass, is a well-documented erosional hot spot characterized by a persistent sand deficit because of the net southward longshore transport (Elko et al., 2005; Elko and Wang, 2007). The main cause of erosion at Upham Beach is its proximal location to Blind Pass, which impounds nearly the entire sand supply from southward longshore transport during a typical dredging interval (4–7 years). The beach south of Upham Beach tends to be accretionary, as the erosional hotspot serves as a feeder beach supplying sand to the downdrift coast (Elko and Wang, 2007).

The morphological characteristics of John's Pass include the distinct channel-margin linear bar along the updrift side of the inlet, the large southward skewed ebb-tidal delta with numerous swash bars, and the apparent downdrift attachment point. The beach north and updrift of John's Pass has been relatively stable over the last decade. Sunshine Beach, south and downdrift of John's Pass, has shown an erosive trend over the years, driven by a reversal of the regional southward longshore transport induced by wave refraction over the John's Pass ebb-tidal delta. The beach at and south of the John's Pass attachment point is accretionary, benefiting from the sand bypassing the ebb-tidal delta. Compared to the inlet morphology of Blind Pass, John's Pass morphological features reflect a substantial influence of the much stronger tidal forcing.

4.3. Calculated tidal currents and waves

The numerical model provides a regional scope to examine the flow, wave, and sediment transport fields, which cannot be obtained from point measurements in the field. Because morphological changes are strongly controlled by temporal and spatial variation (i.e., gradients) in hydrodynamics and sediment transport, flow and wave fields provide insight into the morphological trends. For

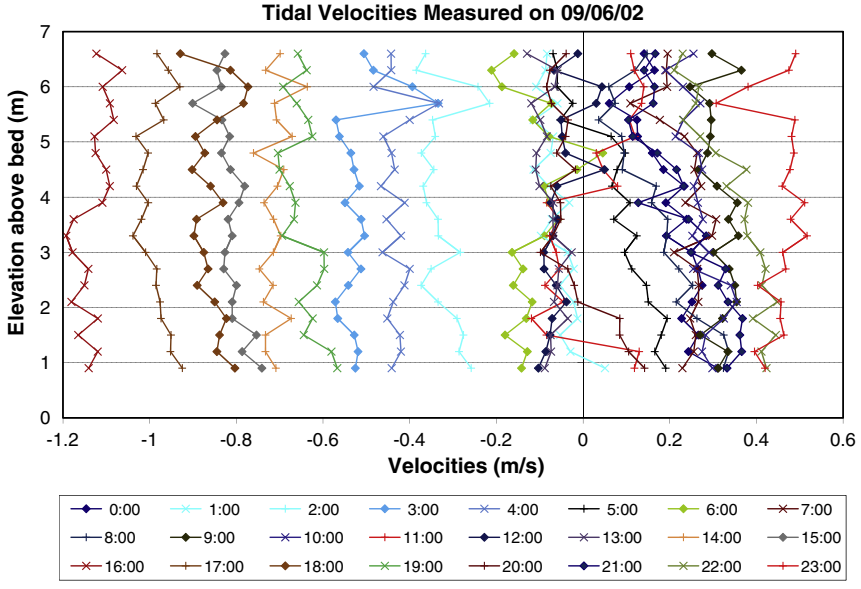

Fig. 11. An example profile of velocity through the water column measured during one tidal cycle over the channel thalweg at Blind Pass. The velocities are largely uniform throughout the water column above roughly 1 m from the bed. Note that ebb velocity (negative) is greater than the flood velocity (positive).

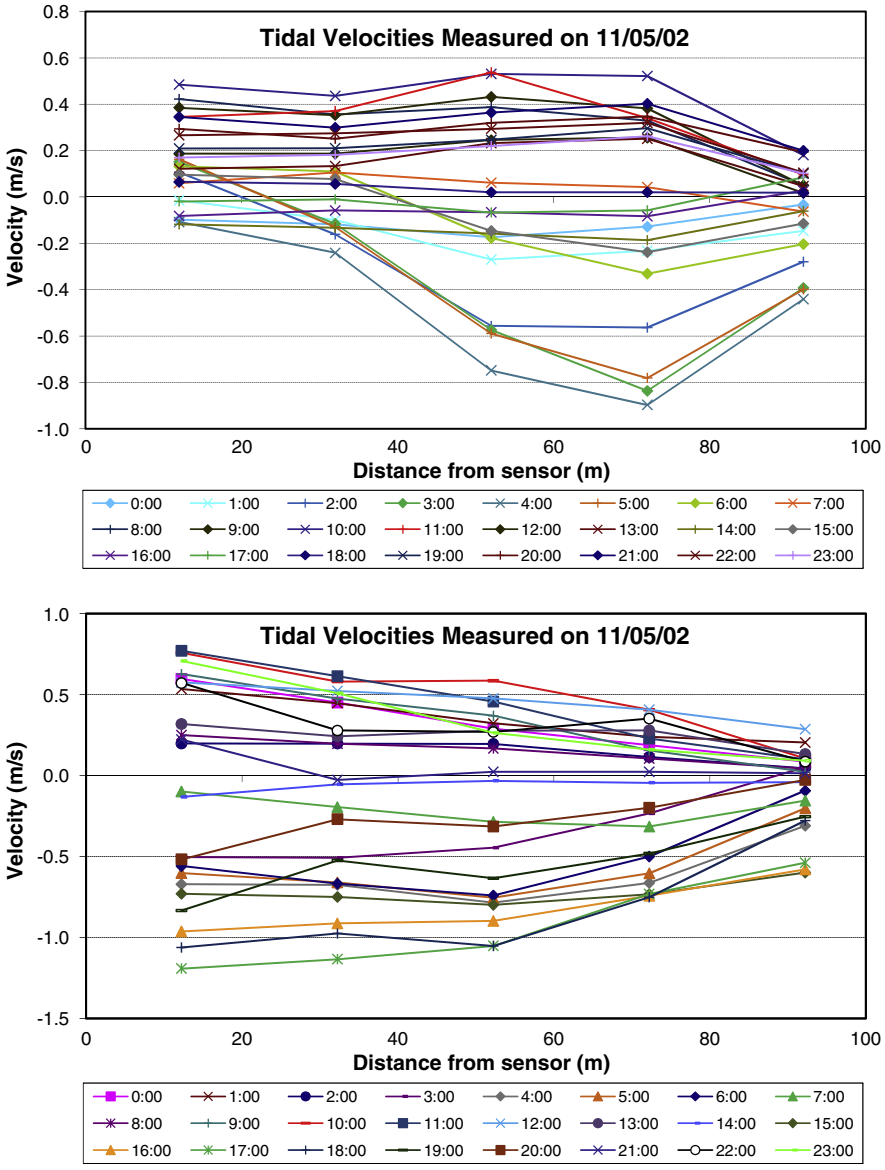

Fig. 12. Examples of velocity distribution across Blind Pass channel. The locations of the gages are shown in Fig. 8. Upper: Velocity distribution measured in the middle section of the inlet. Note that the ebb flow (negative) is much greater than the flood flow (positive) over the channel thalweg. Lower: Velocity distribution measured at the bend in the channel. Note the decreasing velocity toward the bend.

example, as discussed above, the 90-degree turn of Blind Pass resulted in strong ebb flow (~1 m/s) along the southeast side of the inlet and weak ebb flow (~0.4 m/s) along the northwest side, whereas the flood flow is rather uniform across the entire inlet (Figs. 11 and 12). This tidal flow pattern is responsible for the preferential sedimentation in the channel.

The tidal flow patterns, as computed by the CMS model, differ between the mixed-energy John's Pass and the wave-dominated Blind Pass. Strong flows of up to 1.2 m/s are modeled through the entire John's Pass channel during both flood and ebb phases. The ebb jet, which is important for the formation of the ebb-tidal delta, as discussed further in the following, extends to about 1 km offshore. The tidal flow at Blind Pass, by contrast, is considerably weaker and strongly influenced by the 90-degree turn. The flood flow is relatively weak and largely uniform across the entire inlet channel. This contrasts with the ebb flow, which is focused along the south side of the inlet with much larger velocities than the flood flow. Along the north side of the inlet, the ebb flow is quite weak. The modeled pattern agrees well with the measured flow pattern (Fig. 12). The ebb jet, extending along the south side, is rather narrow and extends less than 400 m seaward. The CMS model thus reproduced the John's Pass dominance in terms of tidal flow well.

Regional patterns of wave propagation and wave–current interaction are crucial to sediment transport and therefore morphological change at John's Pass and Blind Pass. Spatial patterns of hydrodynamic forcing are very difficult to measure in the field and therefore are typically inferred from point measurements. Here we attempt to illustrate regional patterns of wave–current interaction and sediment transport semi-quantitatively using the CMS.

Based on field measurements, Wang et al. (2007) suggested that the frequent passage of winter cold fronts and the associated high waves from the north are the dominant mechanisms driving morphological change, as also discussed in Davis (1997). In the following, the calculated interactions of high waves from the north

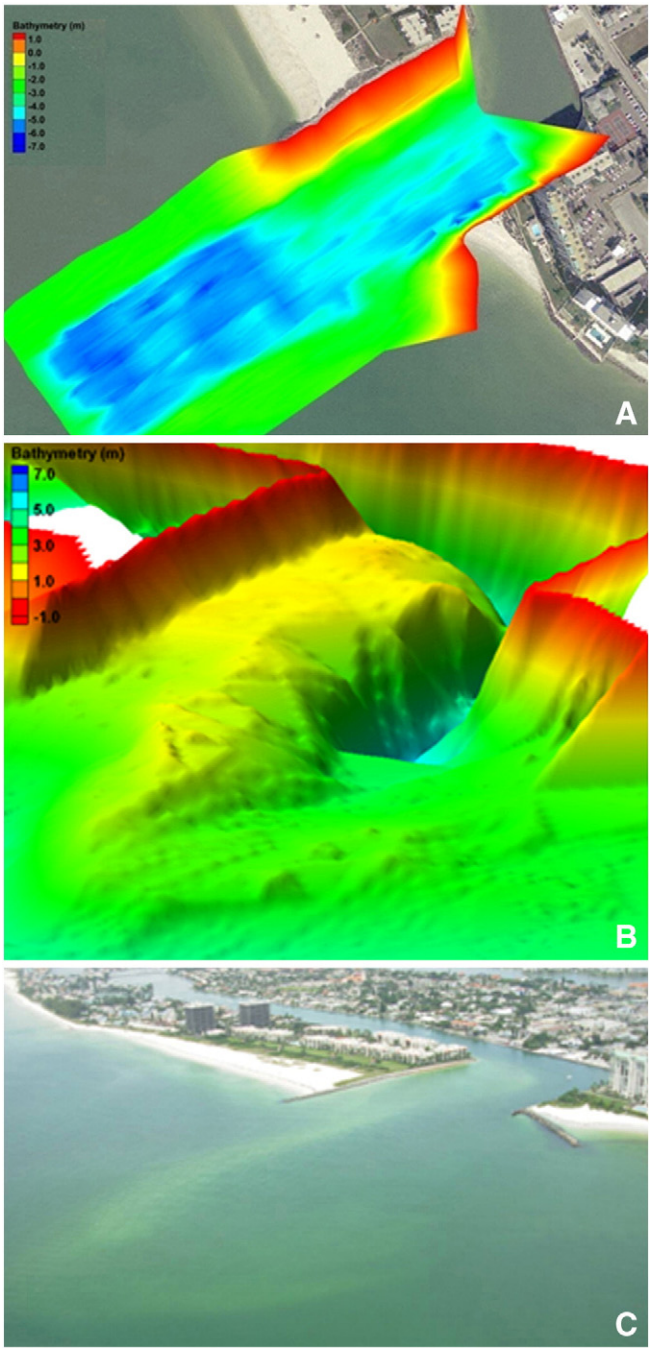

Fig. 13. Ebb-tidal delta development at Blind Pass after the dredging in 2000. *Top*: bathymetry (positive relative to mean sea level) measured immediately after the dredging; *middle*: bathymetry measured in 2008; *bottom*: oblique aerial photo of the ebb-tidal delta taken in July 2008.

and peak flood and ebb currents at both John's Pass and Blind Pass are discussed as a representative key example illustrating the morphodynamics driven by cold fronts.

Under conditions of high waves approaching from the north typically associated with the passage of a cold front, a strong southward wave-driven current is modeled in the nearshore zone and over the John's Pass ebb-tidal delta. Interaction of the longshore current with the flood current leads to the formation of a large eddy downdrift of the inlet, resulting in a current reversal at the chronically eroding Sunshine Beach (Fig. 15). This quantifies and illustrates the classical understanding of wave refraction over ebb deltas and the formation of drum-stick barrier islands (Hayes, 1979; Davis and Hayes, 1984), and further demonstrates that this particular mechanism occurs mostly during the flooding tide. A strong wave-generated current was computed over the ebb lobe, providing the mechanism for sediment bypassing.

Under peak ebb flow, the southward longshore current along the updrift beach is blocked by the strong ebb jet, forming a large eddy north of the inlet (Fig. 16). This large eddy provides the mechanism for the development of the channel margin linear bar, a typical feature of tide-dominated and mixed-energy inlets. In other words, the ebb jet needs to be strong enough to block the longshore current in order to form the large eddy. A strong southward longshore current and a somewhat broadened ebb jet were modeled along the terminal lobe. This current merges with the nearshore longshore current primarily at the attachment point to provide a pathway for southward sand bypassing, similar to the case of the flooding tide.

The wave–current interaction during the passage of the same modeled cold front at the wave-dominated Blind Pass follows a different pattern from that observed at the mixed-energy John's Pass. Overall, the weak tidal flow is overwhelmed by the strong longshore current that flows across the inlet entrance under both flood (Fig. 17) and ebb (Fig. 18) conditions. The two large eddies resulting from the interaction of the longshore current with strong tidal flow over the active ebb-tidal delta, as computed for the mixed-energy John's Pass, are not observed in the modeling results at Blind Pass because of the weak current along the northern portion of the entrance channel (consistent with field observations) and the lack of an ebb-tidal delta. A strong longshore current, responsible for transporting sediment into the inlet, was calculated around the north jetty during the flooding tide (Fig. 17). The relatively weak ebb jet is deflected by the stronger southward longshore current (Fig. 18), resulting in a broad, strong southerly flow along the downdrift Upham Beach. This circulation pattern corresponds to the strong erosive trend observed at this beach (Elko et al., 2005; Elko and Wang, 2007). The modeled current field thus semi-quantitatively illustrates the domination of wave forcing at Blind Pass.

4.4. Calculated sediment transport

Sediment transport processes at tidal inlets are complex, involving both current and wave forcing. Wave breaking occurs over a large portion of the ebb-tidal delta and along the adjacent shoreline. Breaking waves result in much more active sediment suspension than non-breaking waves (Van Rijn, 1993; Wang, 1998; Wang et al., 1998, 2002a, 2002b). Therefore, sediment suspension and transport induced by wave breaking play a crucial role in inlet morphodynamics. In the following, the same examples as discussed above are used to illustrate calculated sediment transport patterns during the passage of a cold front. The modeled transport employed the empirical relationships described in the Lund-CIRP formula (Larson et al., 2011) for non-cohesive sediment transport.

Comparing the calculated flow field (Fig. 15) and associated sediment transport pattern (Fig. 19) at John's Pass under a flooding tide, the significance of breaking waves on sediment suspension and transport is clearly illustrated. The greatest depth-averaged sediment concentration and rate of sediment transport occur at locations where breaking waves (shallow water) occur in combination with strong currents. For this situation, greater sediment concentrations and rates of sediment transport were predicted in three areas: (1) the nearshore area north of the inlet, (2) over the channel-margin linear bar, and (3) along the terminal lobe of the downdrift portion of the ebb-tidal delta. Although strong flow was predicted through the deep channel thalweg (Fig. 15), relatively lower depth-averaged sediment concentrations and rates of transport were predicted due to the absence of wave breaking. A divergence of sediment transport was calculated at Sunshine Beach directly south of John's Pass, which is

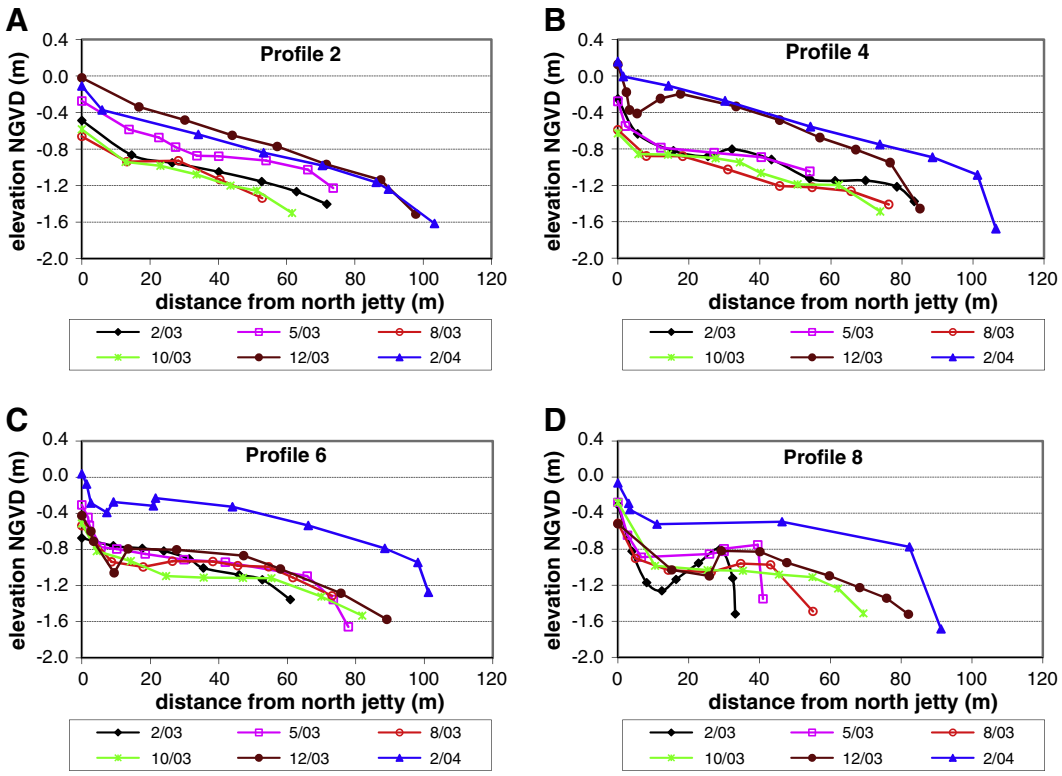

Fig. 14. Profiles from the monthly survey. Locations of the profiles are shown in Fig. 8. Note the sediment accumulation near the inlet entrance at the beginning of the winter season, and sequent landward migration.

responsible for the erosive trend observed there. Sediment bypassing along the terminal lobe of the ebb-tidal delta and on to the beach at the attachment point are related to the longshore current generated by the breaking waves and associated active sediment suspension.

The sediment suspension and transport at John's Pass under peak ebb current (Fig. 20) is substantially different from that of the flood current (Fig. 19). Greater depth-averaged sediment concentrations and rates of sediment transport were calculated in four areas: (1) the nearshore area north of the inlet, (2) the channel margin linear bar and the nearby ebb channel, (3) along the terminal and downdrift lobe of the ebb-tidal delta, and (4) over a broad area of the ebb delta. The active sediment transport in area (1) under both flood and ebb tides is responsible for the littoral sediment supply to the ebb delta. The active transport in area (2) represents sediment flushing by the ebb jet and the development of the channel-margin linear bar. The strongest flow through the channel thalweg does not correlate with the greatest sediment concentration due to the lack of active sediment suspension due to wave breaking. Similar to the flood tide case, the active sediment transport in area (3) provides the mechanism for sand bypassing across the inlet. The active sediment transport in area (4) illustrates the formation of the ebb-tidal delta in a general way.

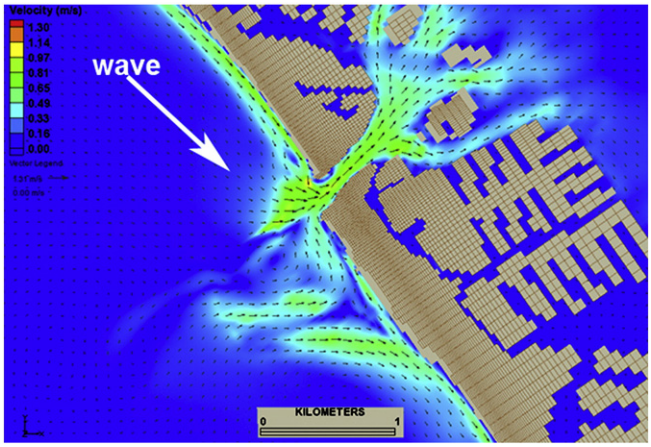

Fig. 15. Calculated wave–current interaction at John's Pass, under a high northerly approaching (arrow) wave with $H_s = 1.9$ m and $T_p = 7.7$ s, during a peak flooding tide. Note the divergent current due to wave refraction in the vicinity of the attachment point.

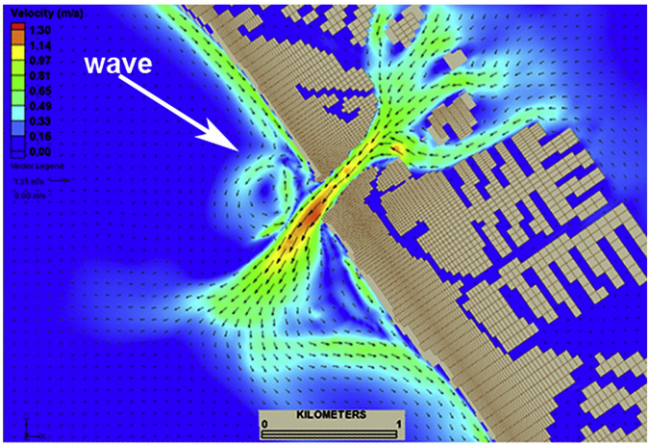

Fig. 16. Calculated wave–current interaction at John's Pass, under a high northerly approaching (arrow) wave with $H_s = 2.0$ m and $T_p = 6.1$ s, during a peak ebbing tide. Note the large eddy developed at the converging longshore current and the ebb jet, which is likely responsible for the development of the channel margin linear bar.

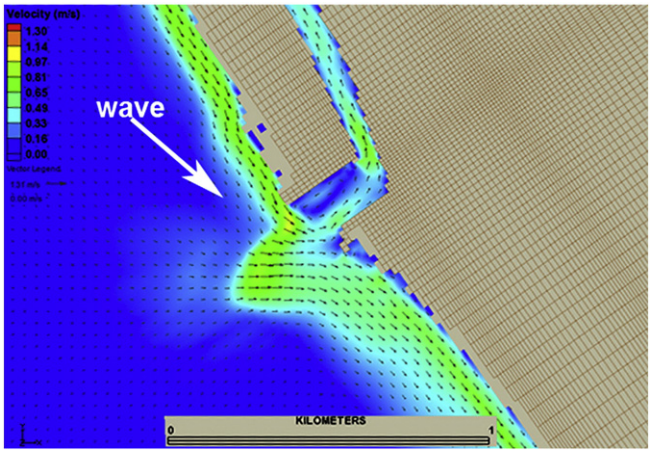

Fig. 17. Calculated wave–current interaction at Blind Pass, under a high northerly approaching (arrow) wave with $H_s = 1.9$ m and $T_p = 7.7$ s, during a peak flooding tide. Note that the relatively weak tidal flow is overwhelmed by the strong longshore current.

In summary, the numerical modeling results suggest that a particular morphological feature in the inlet system behaves differently during different phases of the tide. For example, the channel-margin linear bar tends to be accretional during the ebbing tide but erosive during the flooding tide. The downdrift longshore sediment transport tends to be more active during the flooding tide than during the ebbing tide when it is sheltered by the ebb jet.

At Blind Pass, under peak flood flow (Fig. 21), greater depth-averaged sediment concentrations and transport rates were calculated in three areas: (1) along the Sunset Beach north of the inlet, (2) over the newly developed ebb-tidal delta, and (3) along the downdrift Upham Beach. Active sediment transport in areas (1) and (2) contributes to sedimentation in the inlet channel. The erosion along the updrift Sunset Beach and downdrift Upham Beach corresponds to the active transport in areas (1) and (3). It is worth noting that the calculated sediment transport pattern is based on the bathymetry of 2008 when substantial ebb-tidal delta development occurred at Blind Pass, influenced by the artificial sediment supplies from recent beach nourishments. Without the artificial sediment supply, the ebb delta may not have developed or been maintained. Fairly active sediment bypassing over the developing ebb delta is predicted by the model. It

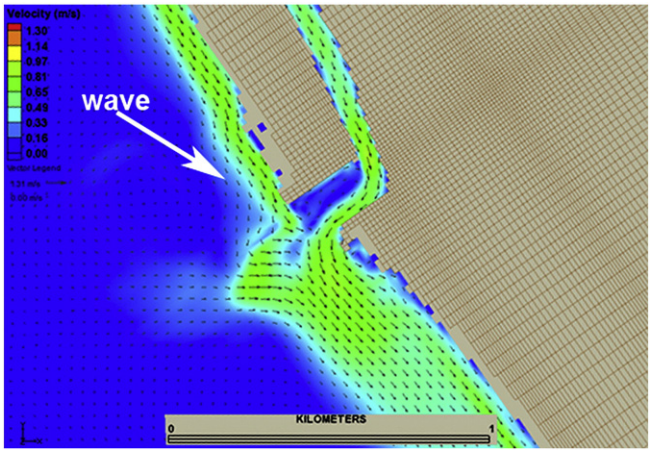

Fig. 18. Calculated wave–current interaction at Blind Pass, under a high northerly approaching (arrow) wave with $H_s = 2.0$ m and $T_p = 6.1$ s, during a peak ebbing tide. Note that the relatively weak tidal flow is overwhelmed by the strong longshore current. Strong current is calculated along the downdrift beach, which is likely responsible for the chronic erosion measured there.

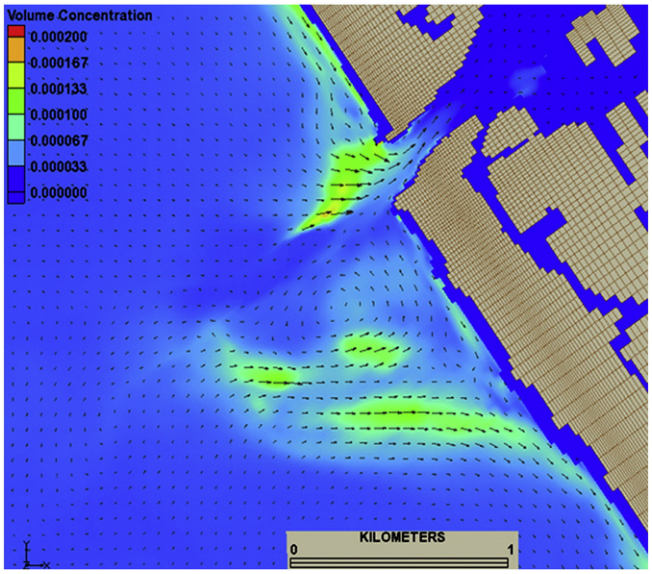

Fig. 19. Calculated depth-averaged sediment volume concentration (dimensionless) and transport vectors at John's Pass, under a high northerly approaching wave with $H_s = 1.9$ m and $T_p = 7.7$ s, during a peak flooding tide. Note the elevated sediment concentration over the shallow part of the ebb delta, indicating the active sediment suspension by breaking waves.

is questionable, however, whether this trend could be maintained at a wave-dominated inlet without artificial sediment supply.

During a peak ebb tide, elevated sediment concentrations and transport rates were predicted in two areas (Fig. 22), the updrift Sunset Beach and extending into the inlet, and across the main ebb channel and along the downdrift Upham Beach. The weak ebb current along the northern side of the inlet is not capable of flushing the sediment deposited during the flood tide. The southward deflected ebb jet, in addition to the strong longshore current, resulted in intensified southward longshore transport along Upham Beach (Fig. 22). This pattern is also interpreted from field observations

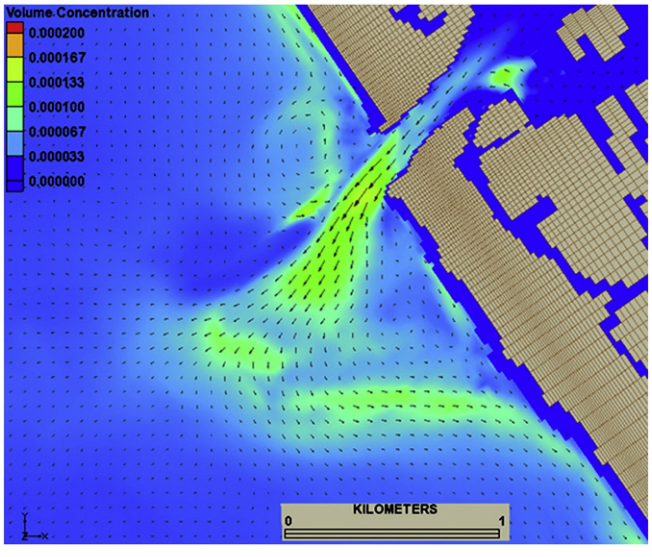

Fig. 20. Calculated depth-averaged sediment volume concentration (dimensionless) and transport vectors at John's Pass, under a high northerly approaching wave with $H_s = 2.0$ m and $T_p = 6.1$ s, during a peak ebbing tide. Note the elevated sediment concentration over the shallow part of the ebb delta, indicating the active sediment suspension by breaking waves. The converging sediment flux along the north side of the inlet channel is likely responsible for the development of the channel margin linear bar.

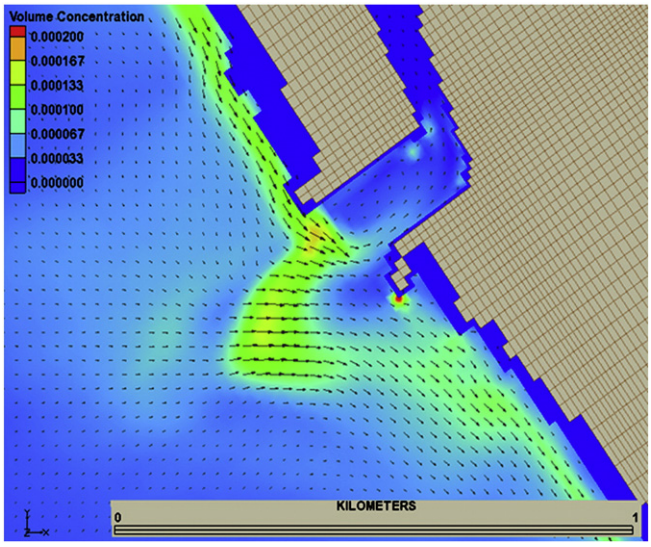

Fig. 21. Calculated depth-averaged sediment volume concentration (dimensionless) and transport vectors at Blind Pass, under a high northerly approaching wave with $H_s = 1.9$ m and $T_p = 7.7$ s, during a peak flooding tide. Note the active sediment transport into the inlet, which is responsible for the deposition measured along the north side.

(Wang et al., 2007). Overall, the calculated sediment transport patterns can be used to interpret several key morphological trends.

5. Conclusions

The co-existence of the dual John's Pass and Blind Pass is realized by the dominance of John's Pass in terms of the tidal prism and size of the ebb delta, and the artificial maintenance of Blind Pass. John's Pass adopts the morphology of a mixed-energy straight inlet with a large, southward skewed ebb-tidal delta, whereas Blind Pass is an artificially stabilized and maintained wave-dominated inlet. Due to the secondary role of Blind Pass, the aggressive anthropogenic activities there do not seem to have a significant influence on the dominating John's Pass. On the other hand, the opening and subsequent evolution of John's Pass had significant influence on the morphodynamics of Blind Pass, causing a sizeable decrease of the tidal prism and a rapid southward migration. In addition, anthropogenic activities had much more influence on the morphodynamics of the more delicate Blind Pass than the more stable John's Pass.

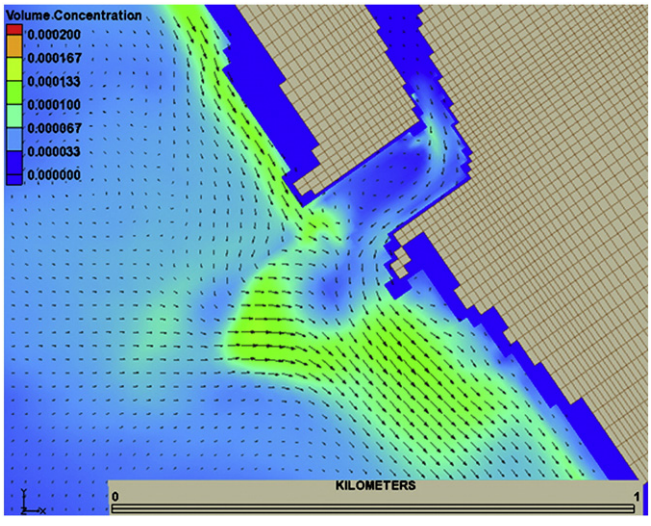

Fig. 22. Calculated depth-averaged sediment volume concentration (dimensionless) and transport vectors at Blind Pass, under a high northerly approaching wave with $H_s = 2.0$ m and $T_p = 6.1$ s, during a peak ebbing tide. Note the elevated longshore transport along the downdrift beach, which is likely responsible for the chronic erosion measured there.

Existing studies and field observations have shown that the morphodynamics of the west-central Florida inlets are substantially influenced by the frequent passages of winter cold fronts. Results from the numerical model, CMS, provide a semi-quantitative understanding and illustration of the morphodynamics of the mixed-energy John's Pass and the wave-dominated Blind Pass in association with cold front passages. A large eddy is modeled from the interaction between the ebb jet and the southward longshore current at John's Pass. This eddy is responsible for the development of the channel-margin linear bar. The interaction between flood flow and southward longshore current results in a large eddy updrift of the attachment point, which is responsible for longshore transport divergence commonly observed downdrift of a mixed-energy tidal inlet. The breaking-induced longshore current and elevated sediment suspension along the ebb delta terminal lobe provide the pathway for sediment bypassing. The morphodynamics of Blind Pass, by contrast, are dominated by wave forcing. The weak ebb jet is not capable of forming a sizable ebb delta and tends to be deflected by the strong longshore current, causing elevated longshore transport along the downdrift beach. The 90-degree turn of the inlet, which is common for wave-dominated migratory inlets, results in weak ebb flushing along the updrift (north) side of the inlet, which was responsible for the historical migration of the inlet before the artificial stabilization, and presently the sedimentation along the north side of the inlet following stabilization.

Acknowledgments

This study was supported by US Army Engineer Research and Development Center's (ERDC) Coastal Inlet Research Program (CIRP), Pinellas County Florida, and the University of South Florida. Permission was granted by Headquarters, U.S. Army Corps of Engineers, to publish this information.

References

Aubrey, D.G., Giese, G.S., 1993. Formation and evolution of multiple tidal inlets. Coastal and Estuarine Studies, No. 44. American Geophysical Union. 237 pp.
Barnard, P.L., 1998. Historical Morphodynamics of Inlet Channels: West-Central Florida. MS thesis, Department of Geology, University of South Florida, Tampa, Florida, 179 pp.
Beck, T.M., Kraus, N.C., 2011. New ebb tidal delta at an old inlet, New Jersey. Journal of Coastal Research, Special Issue 59, 98–111.
Bruun, P., 1978. Stability of Tidal Inlet: Theory and Engineering. Elsevier Scientific Publishing Company, Amsterdam. 510 pp.
Buttolph, A.M., Reed, C.W., Kraus, N.C., Ono, N., Larson, M., Camenen, B., Hanson, H., Wamsley, T., Zundel, A.K., 2006. Two-Dimensional Depth-Averaged Circulation Model CMS-M2D: Version 3.0, Report 2, Sediment Transport and Morphology Change. ERDC/CHL TR-06-9. U.S. Army Engineer Research and Development Center, Vicksburg, MS. 149 pp.
Camenen, B., Larson, M., 2007. A Unified Sediment Transport Formulation for Coastal Inlet Application. ERDC/CHL CR-07-1. U.S. Army Engineer Research and Development Center, Vicksburg, MS. 231 pp.
Davis, R.A., 1994. Barriers of the Florida Gulf Peninsula. In: Davis, R.A. (Ed.), Geology of Holocene Barrier Island Systems. Springer-Verlag, pp. 167–206.
Davis, R.A., 1997. Regional coastal morphodynamics along the United States Gulf of Mexico. Journal of Coastal Research 13, 595–604.
Davis, R.A., Barnard, P.L., 2000. How anthropogenic factors in the back-barrier area influence tidal inlet stability: examples from the Gulf Coast of Florida, U.S.A. In: Pye, K., Allen, J.R.L. (Eds.), Coastal and Estuarine Environments: Sedimentology, Geomorphology and Geoarchaeology, 175. Geological Society London Special Publication, pp. 293–303.
Davis Jr., R.A., Barnard, P., 2003. Morphodynamics of the barrier-inlet system, west-central Florida. Marine Geology 200, 77–101.
Davis, R.A., Hayes, M.O., 1984. What is a wave-dominated coast? Marine Geology 60, 313–329.
Dean, R.G., 1988. Sediment interaction at modified coastal inlets: processes and policies. Lecture Notes on Coastal and Estuarine Studies, 29. Springer-Verlag, Berlin Heidelberg New York Tokyo, pp. 412–439.

Elko, N.A., Wang, P., 2007. Immediate profile and planform evolution of a beach nourishment project with hurricane influences. Coastal Engineering 54, 54–79.
Elko, N.A., Holman, R.A., Gelfenbaum, G., 2005. Quantifying the rapid evolution of a nourishment project with video imagery. Journal of Coastal Research 21, 633–645.
FitzGerald, D.M., 1984. Interactions between the ebb-tidal delta and landward shoreline — price inlet, South-Carolina. Journal of Sedimentary Petrology 54, 1303–1318.
FitzGerald, D.M., 1993. Origin and stability of tidal inlets in Massachusetts. In: Aubrey, D.G., Giese, G.S. (Eds.), Formation and Evolution of Multiple Tidal Inlet Systems. Coastal and Estuarine Studies, No. 44. American Geophysical Union, pp. 1–61.
FitzGerald, D.M., 1996. Geomorphic variability and morphologic and sedimentologic controls on tidal inlets. Journal of Coastal Research 23, 47–71.
FitzGerald, D.M., 2011. Morphodynamics and facies architecture of tidal inlets and tidal deltas. In: Davis, R.A., Dalrymple, R.W. (Eds.), Principles of Tidal Sedimentology. Springer-Verlag, New York Berlin Heidelberg.
Gibeaut, J.C., 1991. Morphodynamic classification, evolution, and modeling of unstructured inlets in west-central Florida. Ph.D. dissertation, Department of Marine Science, University of South Florida. 192 pp.
Hayes, M.O., 1979. Barrier island morphology as a function of tidal and wave regimes. In: Leatherman, S.P. (Ed.), Barrier Islands: From the Gulf of St. Lawrence to the Gulf of Mexico. Academic Press, New York, pp. 1–27.
Kraus, N.C., 2009. Engineering of tidal inlets and morphologic consequences. In: Kim, Y.C. (Ed.), Handbook of Coastal and Ocean Engineering. World Scientific, Singapore, pp. 867–901.
Kraus, N.C., Militello, A., 1999. Hydraulic study of multiple inlet system: East Matagorda Bay, Texas. Journal of Hydraulic Research 125, 224–232.
Larson, L., Camenen, B., Nam, P.T., 2011. A unified sediment transport model for inlet application. Journal of Coastal Research, Special Issue 59, 27–39.
Lin, L., Mase, H., Yamada, F., Demirbilek, Z., 2006. Wave Action Balance Equation Diffraction (WABED) Model: Tests of Wave Diffraction and Refraction at Inlets. ERDC/CHL CHETN-III-3. U.S. Army Engineer Research and Development Center, Vicksburg, MS. 24 pp.
Lin, L., Demirbilek, Z., Mase, H., Zheng, J., Yamada, F., 2008. CMS-Wave: A Nearshore Spectral Model for Coastal Inlets and Navigation Projects. ERDC/CHL TR-08-13. U.S. Army Engineer Research and Development Center, Vicksburg, MS. 120 pp.
Lin, L., Demirbilek, Z., Mase, H., 2011. Recent capabilities of CMS-Wave: a coastal wave model for inlets and navigation projects. Journal of Coastal Research, Special Issue 59, 7–15.
Mase, H., 2001. Multidirectional random wave transformation model based on energy balance equation. Coastal Engineering Journal (JSCE) 43, 317–337.
Mase, H., Kitano, T., 2000. Spectrum-based prediction model for random wave transformation over arbitrary bottom topography. Coastal Engineering Journal (JSCE) 42, 111–151.
Mase, H., Oki, K., Hedges, T.S., Li, H., 2005. Extended energy-balance-equation wave model for multidirectional random wave transformation. Ocean Engineering 32, 961–985.
Mehta, A.J., Adams, W.D., Jones, C.P., 1976. John's Pass and Blind Pass: Glossary of Inlets Report Number 4. Florida Sea Grant Program, Report Number 18. 66 pp.
Pacheco, A., Ferreira, O., Williams, J.J., Garel, E., Vila-Concejo, A., Dias, J.A., 2010. Hydrodynamics and equilibrium of a multiple-inlet system. Marine Geology 274, 32–42.
Reed, C.W., Brown, M.E., Sanchez, A., Wu, W., Buttolph, A.M., 2011. The Coastal Modeling System Flow Model (CMS-Flow): past and present. Journal of Coastal Research, Special Issue 59, 1–7.
Salles, P., Voulgaris, G., Aubrey, D., 2005. Contribution of nonlinear mechanisms in the persistence of multiple tidal inlet systems. Estuarine Coastal and Shelf Science 65, 475–491.
Sanchez, A., Wu, W., 2011. A non-equilibrium sediment transport model for coastal inlets and navigation channels. Journal of Coastal Research, Special Issue 59, 39–49.
Tanner, W.F., 1960. Florida coastal classification. Transactions — Gulf Coast Association of Geological Science 10, 259–266.
Van de Kreeke, J., 1990. Can multiple inlets be stable? Estuarine Coastal and Shelf Science 30, 261–273.
Van de Kreeke, J., Brouwer, R.L., Zitman, T.J., Schuttelaars, H.M., 2008. The effect of a topographic high on the morphological stability of a two-inlet bay system. Coastal Engineering 55, 319–332.
Van Rijn, J.C., 1993. Principles of Sediment Transport in Rivers, Estuaries and Coastal Seas. Aqua Publications, the Netherlands. 831 pp.
Walton Jr., T.L., 1973. Littoral drift computations along the coast of Florida by means of ship wave observations. Coastal and Oceanographic Engineering Laboratory Technical Report No. 15. University of Florida, Gainesville, Florida. 80 pp.
Wang, P., 1998. Longshore sediment flux in the water column and across the surf zone. Journal of Waterway, Port, Coastal & Ocean Engineering, ASCE 124, 108–117.
Wang, P., Kraus, N.C., Davis Jr., R.A., 1998. Total rate of longshore sediment transport in the surf zone: field measurements and empirical predictions. Journal of Coastal Research 14, 269–283.
Wang, P., Smith, E.R., Ebersole, B.A., 2002a. Large-scale laboratory measurements of longshore sediment transport under spilling and plunging breakers. Journal of Coastal Research 18, 118–135.
Wang, P., Ebersole, B.A., Smith, E.R., Johnson, B.D., 2002b. Temporal and spatial variations of surf-zone currents and suspended-sediment concentration. Coastal Engineering 46, 175–211.
Wang, P., Tidwell, D.K., Beck, T.M., Kraus, N.C., 2007. Sedimentation patterns in a stabilized migratory inlet, Blind Pass, Florida. Proceedings of Coastal Sediments 07. ASCE Press, pp. 1377–1390.
Wang, P., Roberts, T.M., Elko, N.A., Beck, T.M., 2008. Factors controlling the first year performance of eight adjacent beach nourishment projects, west-central Florida, USA. Proceedings of the 31st International Conference on Coastal Engineering. World Scientific, Singapore, pp. 2532–2544.
Wu, W., 2008. Computation River Dynamics. Taylor and Francis, London. 589 pp.
Wu, W., Sanchez, A., Zhang, M., 2011. An implicit 2-D shallow water flow model for inlets and navigation projects. Journal of Coastal Research, Special Issue 59, 15–27.